

## Electronic Supplementary Information

### **Van der Waals solid solution crystals for highly efficient in-air photon upconversion under subsolar irradiance**

Riku Enomoto,<sup>a</sup> Megumi Hoshi,<sup>a</sup> Hironaga Oyama,<sup>b</sup> Hideki Agata,<sup>c</sup> Shinichi Kurokawa,<sup>d</sup> Hitoshi Kuma,<sup>d</sup> Hidehiro Uekusa,<sup>b</sup> and Yoichi Murakami<sup>a,e\*</sup>

<sup>a</sup> School of Engineering, Tokyo Institute of Technology, 2-12-1 Ookayama, Meguro-ku, Tokyo 152-8552, Japan.

<sup>b</sup> Department of Chemistry, School of Science, Tokyo Institute of Technology, 2-12-1 Ookayama, Meguro-ku, Tokyo 152-8552, Japan.

<sup>c</sup> Nissan Motor Co., Ltd., 2 Takaracho, Kanagawa-ku, Yokohama, Kanagawa 220-8623, Japan.

<sup>d</sup> Idemitsu Kosan Co., Ltd., 1-2-1 Otemachi, Chiyoda-ku, Tokyo 100-8321, Japan.

<sup>e</sup> PRESTO, JST, 4-1-8 Honcho, Kawaguchi, Saitama 332-0012, Japan.

\*Corresponding Author. E-mail: murakami.y.af@m.titech.ac.jp

## **List of Contents**

- 1. Experimental section**
- 2. Experimental setup for optical absorption measurements (Fig. S1)**
- 3. Optical micrographs at high magnification (Fig. S2)**
- 4. Polarization-dependent optical absorption measurements (Fig. S3)**
- 5. Experimental setup for photoemission measurements (Fig. S4)**
- 6. Reference sample prepared with DPA (Fig. S5)**
- 7. All data for 20 samples measured (Table S1, Figs. S6 and S7)**
- 8. PXRD patterns before and after annealing (Fig. S8)**
- 9. Fluorescence quantum yields of the crystals (Table S2)**
- 10. Fluorescence spectra of ANNP in the solution and crystals (Fig. S9)**
- 11. Experimental setup with a solar simulator and optical filter used (Fig. S10)**
- 12. Thermogravimetric analysis data (Fig. S11)**
- 13. Crystallographic data (Table S3)**
- 14. Comparison of triplet diffusion properties with previous reports (Table S4)**
- 15. Distance between ANNP molecules in the crystal (Fig. S12)**
- 16. Time-resolved fluorescence intensity decay curve for ANNP in solution (Fig. S13)**
- 17. Laser power fluctuation during photostability measurements (Fig. S14)**

**References**

## **Experimental section**

### **Chemicals**

ANNP and DPA were supplied from Idemitsu Kosan and TCI, respectively; both of which were sublimation grade and used as received. PtOEP (95+%) was supplied from Aldrich and the toluene solution ( $1.74 \times 10^{-4}$  M) was passed through a PTFE filter (pore size: 200 nm, Merck-LG, SLLGX13NL) to remove solid particulates. Toluene (99.8+%) and ethanol (99.5+%) were obtained from FUJIFILM Wako Chemicals and used as received.

### **Crystal growth**

As schematically depicted in Fig. 1d, on a hotplate at 80 °C, a toluene solution of PtOEP and ANNP ( $1.74 \times 10^{-4}$  and  $2.0 \times 10^{-2}$  M, respectively) in a glass vial was diluted with hot ethanol at 80 °C until the volume ratio of toluene:ethanol reached 1:3, where ethanol was used as a poor solvent. The solubilities of PtOEP and ANNP in toluene at room temperature were ca.  $8.9 \times 10^{-4}$  and  $2.2 \times 10^{-1}$  M, respectively. Immediately after addition of ethanol, the glass vial was capped and stored on a steel shelf at  $24^\circ\text{C} \pm 2^\circ\text{C}$  in the dark. After 2–3 days, crystals were evident on the bottom of the vial (refer to the photograph in Fig. 1d). The crystals were collected on filter paper under vacuum filtration, during which a small quantity of cold (8°C) toluene was dropped onto the crystals with a Pasteur pipette to lightly wash the surface of the crystals (to prevent possible precipitation of solids by evaporation of the crystal growth solution). All these procedures were conducted in air. The crystals were then dried in an evacuated glass jar for ca. 30 min. The annealing was carried out at 90°C for 4 days in a closed container filled with dry nitrogen gas to ensure reproducibility.

### **Optical absorption measurements of a single crystal**

Optical absorption spectra of a single crystal (e.g., Fig. 2c) were acquired using a microscope setup illustrated by Fig. S1. As depicted, white light generated by an LED lamp was focused on a sample crystal from the bottom of the sample stage. The transmitted light was collected with a 10× objective lens and then guided into a monochromator (Princeton, SP-2300i) through an optical fiber (multimode, core

diameter: 300  $\mu\text{m}$ ). Although the spot diameter of the white light on the crystal was ca. 200  $\mu\text{m}$ , the diameter of the actual probing area on the sample crystal was ca. 40  $\mu\text{m}$ , which was determined by the optics of the light collection path. The spectrum was recorded by an arrayed CCD detector (Princeton, PIXIS:100BR) mounted at the exit of the monochromator. A comparison of the white light spectra acquired with and without the sample crystal yielded an optical absorption spectrum for the ca. 40- $\mu\text{m}$  spot area.

### Photoemission measurements from a single crystal

Acquisition of UC emission spectra from a single crystal was carried out with the setup illustrated by Fig. S4. A large portion of this setup (objective lens, sample stage, monochromator, and CCD) was identical to that used for the optical absorption measurements previously described. As illustrated by Fig. S4, a laser beam at 542 nm was first expanded with a beam expander and only the central part was taken out using an iris. Then, the light was focused onto a sample crystal on the microscope stage. The laser beam had a top-hat intensity profile with a diameter of 50  $\mu\text{m}$  at the sample position (Fig. S4). The photoemission from the sample was collected through the same objective lens and guided into the monochromator through an optical fiber (multimode, core diameter: 182  $\mu\text{m}$ ). The spectrum was recorded with the arrayed CCD. All the photoemission spectra, some of which were used to determine  $\Phi_{\text{UC}}$ , were corrected by the wavelength-dependent sensitivities of the grating and CCD.

### Determination of UC quantum yield $\Phi_{\text{UC}}$

The maximum  $\Phi_{\text{UC}}$  is defined as 50% throughout this report. The value of  $\Phi_{\text{UC}}$  was determined by the following relationship<sup>1</sup>

$$\Phi_{\text{UC}} = \Phi_{\text{Ref}} \left( \frac{1 - 10^{-A_{\text{R}}}}{1 - 10^{-A_{\text{UC}}}} \right) \left( \frac{I_{\text{R}}^{\text{Ex}}}{I_{\text{UC}}^{\text{Ex}}} \right) \left( \frac{h\nu_{\text{UC}}^{\text{Ex}}}{h\nu_{\text{R}}^{\text{Ex}}} \right) \left( \frac{I_{\text{UC}}^{\text{Em}}}{I_{\text{R}}^{\text{Em}}} \right) \left( \frac{n_{\text{UC}}}{n_{\text{R}}} \right)^2, \quad (\text{S1})$$

where  $\Phi$  is photoemission quantum yield,  $A$  is the absorbance at the excitation wavelength,  $I^{\text{Ex}}$  is the excitation intensity,  $h\nu^{\text{Ex}}$  is the photon energy at the excitation wavelength,  $I^{\text{Em}}$  is the emission intensity, and  $n$  is the refractive index. The subscripts ‘‘UC’’ and ‘‘R’’ represent UC sample and reference, respectively. We used an ethylene glycol solution of rhodamine 101 at a concentration of  $1 \times 10^{-6}$  M as the reference, the fluorescence

quantum yield  $\Phi_{\text{Ref}}$  of which was determined to be 89.2% with an absolute photoluminescence quantum yield spectrometer (Hamamatsu, C11347-01). The refractive index of ANNP ( $n_{\text{UC}}$ ) is 1.81 at 450 nm, determined from an ellipsometry measurement of the vacuum-deposited thin film on a glass substrate. The excitation wavelength of 542 nm was commonly used for both the sample and reference, and therefore  $h\nu_{\text{UC}}^{\text{Ex}} = h\nu_{\text{R}}^{\text{Ex}}$ . Because the spectra were acquired with the arrayed CCD and the wavelength sensitivities of both the grating in the monochromator and the CCD were corrected, the spectrally integrated emission intensity was used for  $I_{\text{UC}}^{\text{Em}}$  and  $I_{\text{R}}^{\text{Em}}$ . The identical optical alignment and excitation beam spot size (50  $\mu\text{m}$ ) were used in the measurements of both the sample and reference, which were conducted consecutively in the same experiment.  $A_{\text{R}}$  and  $A_{\text{UC}}$  were acquired using the aforementioned setup, where the reference rhodamine 101 solution was filled between two glass plates with a spacing chosen between 50 and 200  $\mu\text{m}$  (refer to Fig. S1) such that the spacing matched the thickness of a sample crystal under investigation.

#### **Time-resolved measurements of UC emission intensity**

Nanosecond light pulses at 540 nm (pulse duration: ca. 3 ns, repetition rate: 20 Hz) from an optical parametric oscillator (EKSPLA, NT-242) were irradiated onto an ensemble of ca. 10 crystals on a glass slide. The UC fluorescence was collected in the perpendicular direction using a pair of aromatic lenses and then focused onto the entrance slit of a monochromator (Princeton, SP-2300i), the grating position of which was set at 455 nm. The transient intensity signal was acquired with a photomultiplier tube (Hamamatsu, H11461) mounted at the exit of the monochromator.

#### **Time-resolved measurements of fluorescence intensity**

Time-resolved fluorescence intensity decay curves were acquired with a time-correlated single-photon counting (TCSPC) setup using femtosecond light pulses (wavelength: 405 nm, repetition rate: 8 MHz) generated from a Ti-sapphire laser (Spectra Physics, Tsunami). The monitor wavelength was 455 nm. The photons were detected with a microchannel plate photomultiplier tube (Hamamatsu, R3809U-50) mounted at the exit

of a monochromator (Princeton, SP-2150i), followed by signal processing with a photon counting board (Becker & Hickl, SPC-130-EM).

### **Photoemission measurements from ensemble crystals with a solar simulator**

Simulated AM1.5 sunlight was generated with a solar simulator (Asahi Spectra, HAL-320). A photograph of the experimental setup is shown in Fig. S10a. As shown, the simulated AM1.5 light first entered a 510-nm long-pass filter (Asahi Spectra, F02A, size: 50 mm × 50 mm), the transmission and optical density (O. D.) spectra of which are given in Fig. S10b. The filter was placed on a light-absorbing black plate with a square aperture of approximately  $(1.5 \times 1.5) \text{ cm}^2$ . Through this aperture, only the central uniform portion of the light was extracted. The light after the filter, which comprised only wavelengths longer than 510 nm and thus appeared yellowish, was irradiated onto the ensemble of sample crystals (quantity: 3.2 mg) placed on a glass slide, which was mounted on a precision three-axis stage. The photoemission was collected and collimated by this achromatic lens and then focused onto an entrance slit of a monochromator (Princeton, SP-2300i) with another achromatic lens. The spectrum was recorded with an arrayed CCD (Princeton, PIXIS:100BR) and the wavelength-integrated intensity (from 430 to 455 nm) were used as the UC emission intensity shown in Fig. 3e in the main text. The spectrum in the inset of Fig. 3e was corrected by the wavelength-dependent sensitivities of the grating of the monochromator and CCD, similarly to the rest of the photoemission spectra shown in this article. The position of the glass slide was adjusted such that the sample position matched the focal point of the achromatic lens by maximizing the UC emission intensity detected with the CCD system.

As shown in the inset of Fig. 3e in the main text, replacement of the UC crystals by the ANNP powder completely eliminated the photoemission signal, indicating that the blue emission detected by this system was caused by the presence of PtOEP and hence was not an artifact—such as an unexpected down-converted fluorescence. As shown by Fig. S10b, the optical filter had a high O. D. of greater than 5–6 for wavelengths shorter than 490 nm, which was sufficient to block all UV light in the irradiance from the solar simulator.

The optical power at the sample position was carefully set as follows. First, without the long-pass filter, a one-sun checker (Asahi Spectra, CS-20) was placed at the sample position and the irradiation at that position was set to the one-sun intensity. This irradiance was double-checked using a thermal-type power sensor (Ophir, 10A-V1.1), and these results agreed well within 10%. Therefore, we relied on the irradiance values reported by the one-sun checker. Then, the long-pass filter was placed on the aforementioned aperture. Subsequently, because this long-pass filter exhibited a 95% transmittance in the wavelength range of 515–600 nm (Fig. S10b), the irradiance of the solar simulator was increased by 1.05 times to compensate the reduction of the light power at the sample position caused by insertion of this long-pass filter. We defined this state as 1 $\odot$  (one sun) intensity at the sample position. All the data were acquired in the dark to avoid any potential artifacts that could arise from environmental light.

#### **Photostability check under continuous photoirradiation**

Using the same setup as that used for the time-resolved photoemission measurements, an ensemble of ca. 10 crystals on a glass slide (refer to the inset photograph of Fig. 3f in the main text) was continuously irradiated in air with 542-nm laser light of 20-mW cm<sup>-2</sup> intensity, which is ca. one order of magnitude higher intensity than  $I_{th}$  (Fig. S6 and Table S1). The laser beam profile exhibited a top-hat shape (Fig. S4). The UC emission spectra were continuously acquired with a monochromator (Princeton, SP-2300i) and an arrayed CCD detector (Princeton, PIXIS:100BR) with an interval of 10 s, and the spectrally integrated value over 450–460 nm was taken as the UC emission intensity. Temporal fluctuations in the laser power were simultaneously recorded with a digital power meter (Ophir, PD300), with which the temporal fluctuation in the UC emission intensity was linearly corrected (Fig. S14). This correction was justified because the aforementioned excitation condition corresponds to a strong excitation limit, where the UC emission intensity changes linearly in accordance with the excitation power.<sup>2,3</sup>

#### **Thermogravimetric analysis**

Thermogravimetric analysis (TGA) of the samples was carried out with a Thermo Plus EVO2 (Rigaku) under a heating rate of 2°C/min and flowing 400 sccm of dry nitrogen

gas. A typical sample quantity was 4.5 mg. The weight loss was also checked by comparing the weight of the sample before and after TGA with an ultramicro balance (Sartorius, MSA2.7S-000-DM).

### **Single-crystal X-ray diffraction measurements and data analysis**

The measurements were performed with a single-crystal X-ray diffractometer (XtaLAB Synergy-DW, Rigaku, Open Facility Center at Tokyo Institute of Technology) at 93 K with Cu K $\alpha$  radiation (40 kV, 30 mA). Because the UC crystals consist of multiple domains (Fig. 2b in the main text), a single crystalline domain was carefully taken out with a surgical scalpel under a stereomicroscope. The analysis of the data was conducted as follows. The structures were solved by SHELXT 2018/2 (G. M. Sheldrick, *Acta Cryst.*, **2015**, A71, 3–8) and subsequently refined on  $F^2$  with SHELXL 2017/1 (G. M. Sheldrick, *Acta Cryst.*, **2015**, C71, 3–8). All nonhydrogen atoms were refined anisotropically. Hydrogen atoms were placed at the geometrically calculated positions and refined using isotropic thermal parameters set to  $x$ -times those of the parent atoms, where  $x$  is 1.5 (hydroxy and methyl hydrogens of solvent ethanol) or 1.2 (all hydrogens of ANNP). The occupancy of ethanol solvent (ca. 20%, refer also to Table S3) was determined by least-squares refinement with a free variable.

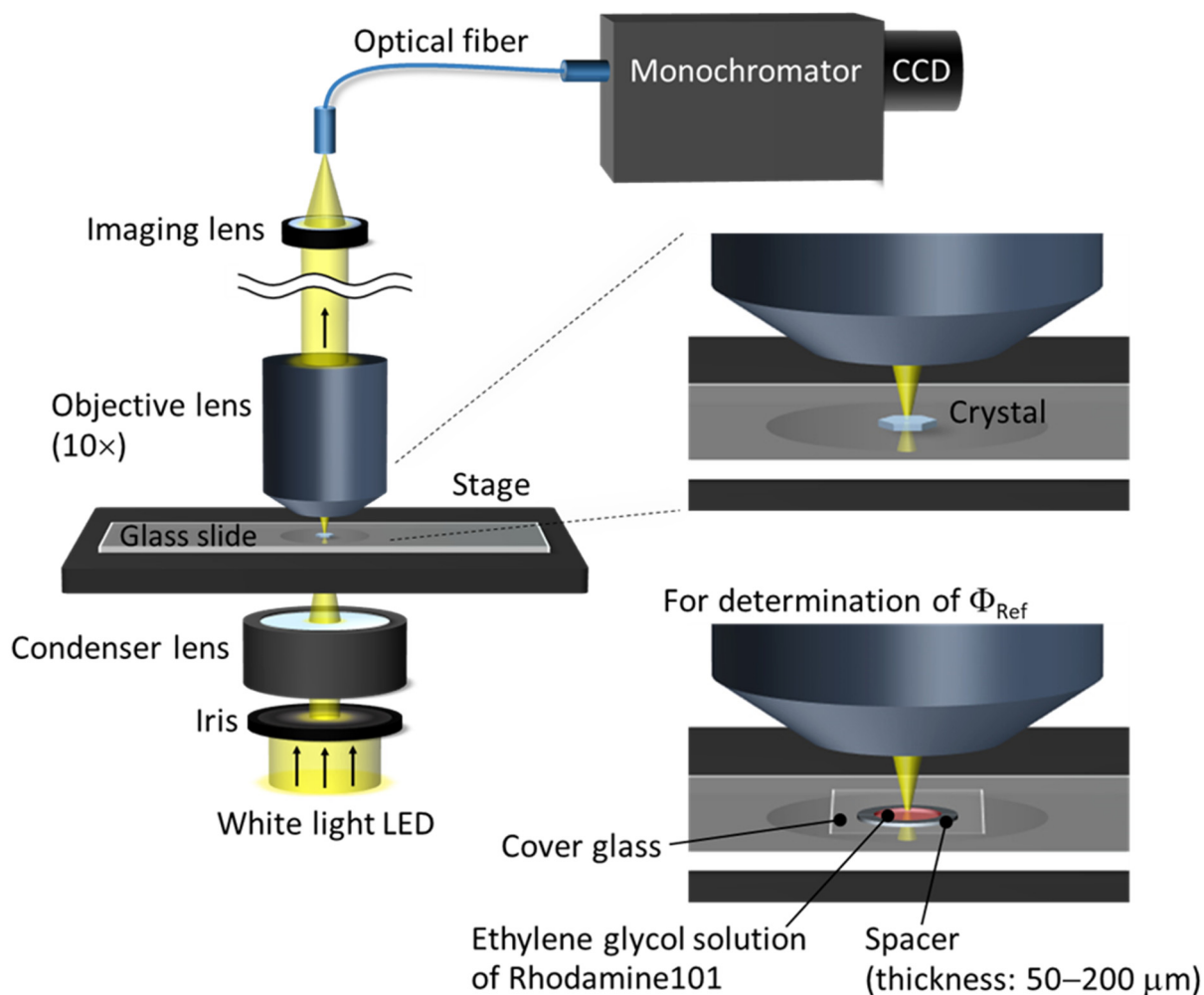


**Fig. S1.** Schematic of the experimental setup used for optical absorption measurements. This system enables acquisition of an optical absorption spectrum from a narrow area with a diameter of ca. 40  $\mu\text{m}$ . When  $\Phi_{Ref}$  in Eq. S1 was determined using an ethylene glycol solution of Rhodamine 101, the thickness of the spacer (a metal sim ring) was selected so that the thickness of the spacer matched the thickness of the UC crystal within  $\pm 15 \mu\text{m}$ .

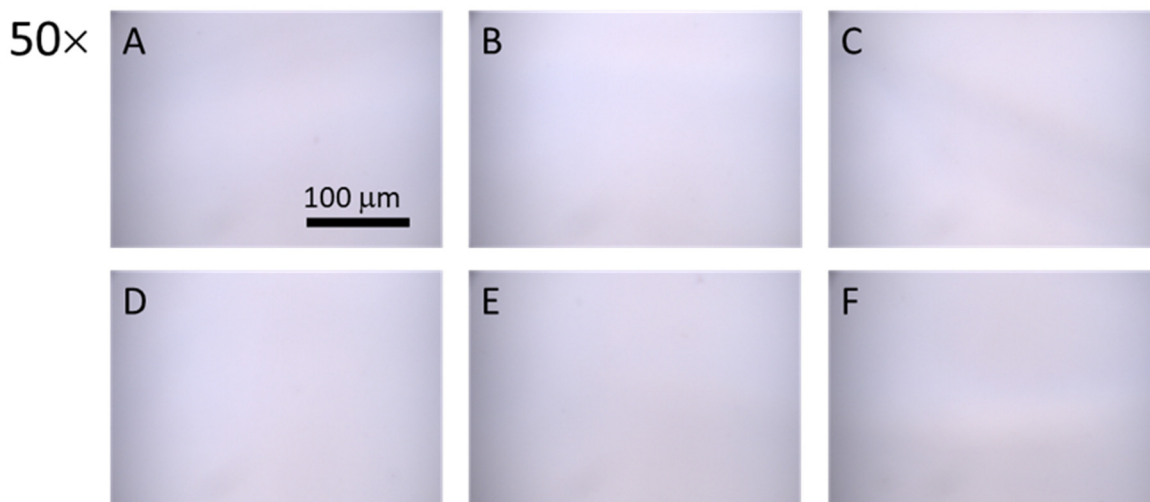
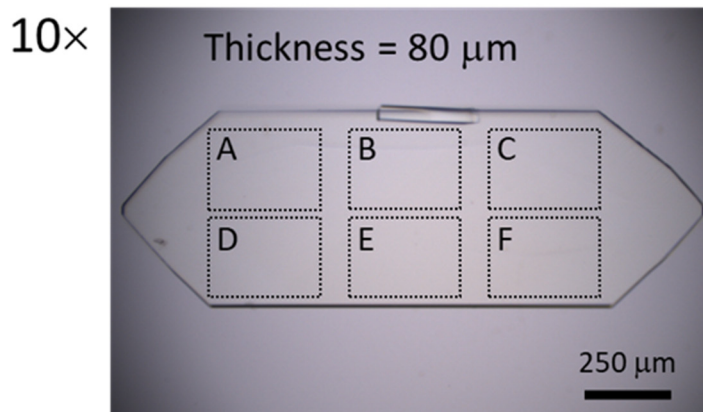


**Fig. S2.** Detailed observations of a UC crystal with an optical microscope. The bottom micrographs, A to F, were acquired at 50× magnification over the regions indicated in the top micrograph. They showed no aggregates on the surface and inside the crystal, which is consistent with the negligibly small phosphorescence from PtOEP shown in the inset of Fig. 3a in the main text.

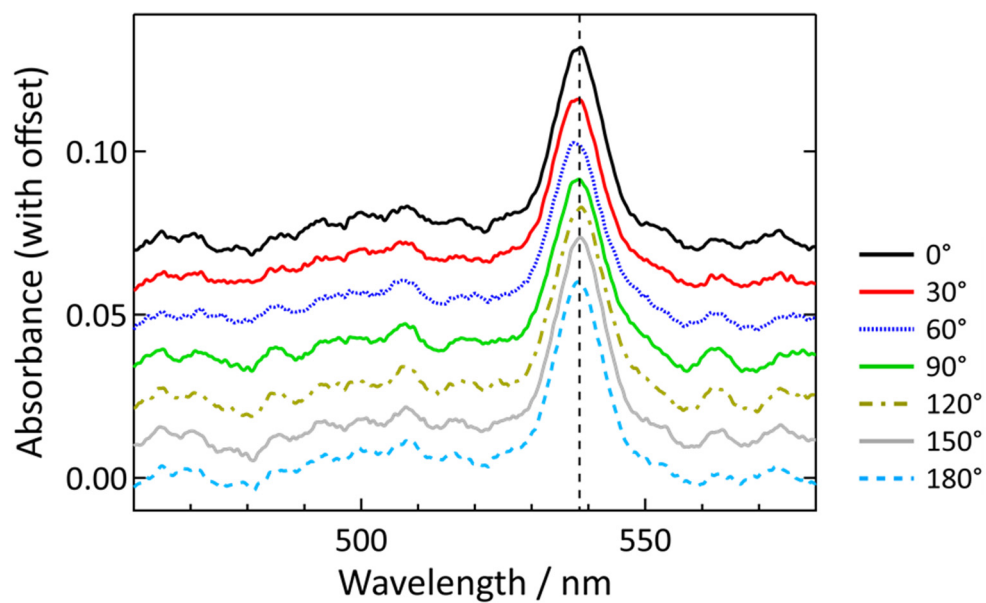
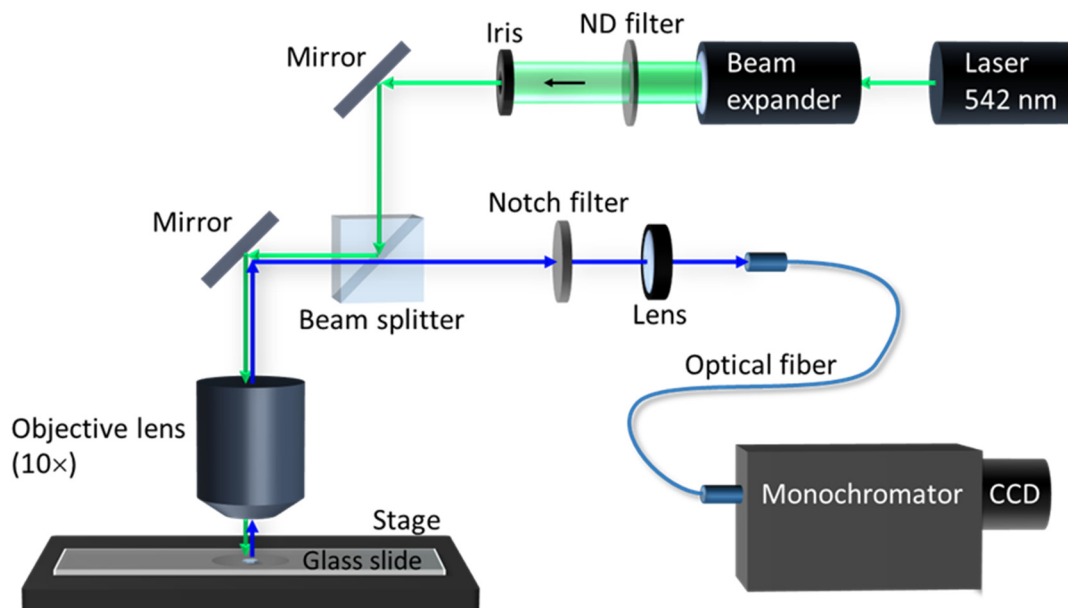
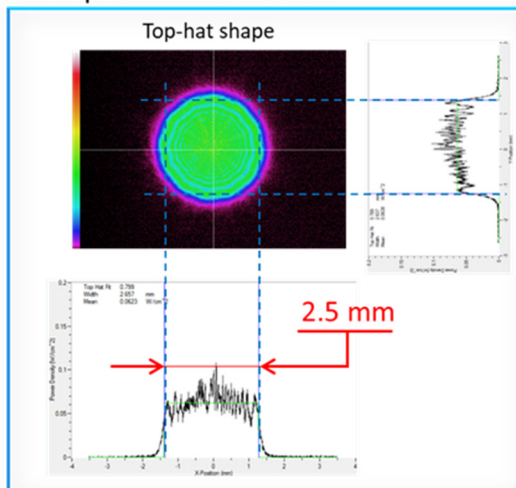


**Fig. S3.** Polarization-dependent optical absorption measurements of a typical sample crystal. Using the measurement setup of Fig. S1, these spectra were acquired by rotating a polarizer placed beneath the sample stage. The results indicate that PtOEP molecules dissolved in an ANNP crystal have no preferential orientation, at least for the direction normal to the largest crystal plane.



Beam profile after the iris:



Beam profile on the stage (sample position):

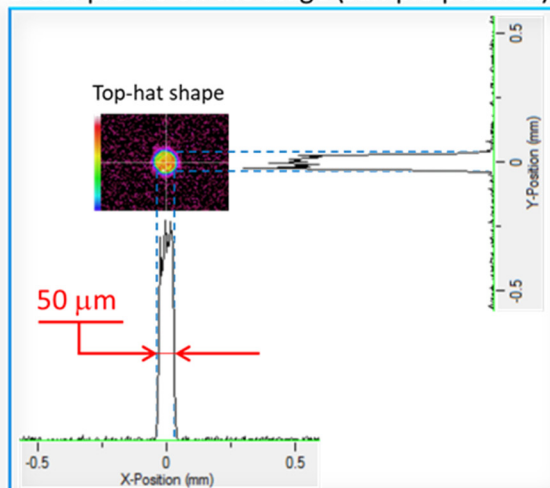


**Fig. S4.** Schematic of the experimental setup used for photoemission measurements. The bottom-left and bottom-right images show the top-hat laser beam profiles after the iris (used for Figs. 3d and 3f in the main text) and on the microscope stage at the sample position (used for Figs. 3a, 3b, and 3c in the main text). Note that a large portion of this setup (objective lens, stage, monochromator, and CCD) is identical to that shown in Fig. S1; these two configurations for absorption and photoemission measurements were concurrently used when  $\Phi_{\text{Ref}}$  and  $\Phi_{\text{UC}}$  were determined.

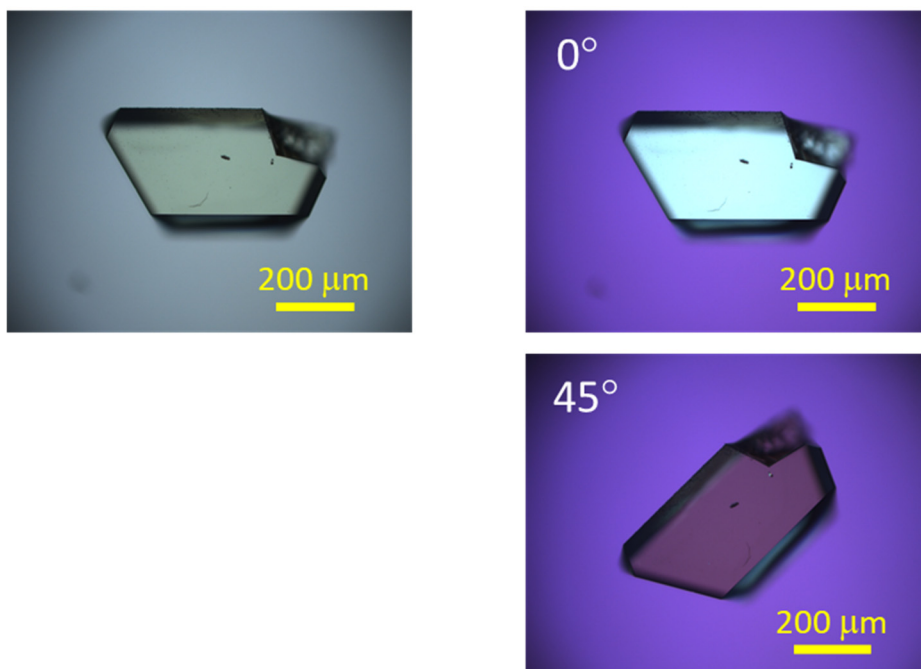


**Fig. S5.** Micrograph of the reference crystal prepared with DPA (left) and its polarized micrograph (right), indicating the single-crystalline nature. This crystal was prepared following the same procedure as that used to prepare the UC crystal with ANNP except that the concentration of DPA in the starting toluene solution was twice ( $4.0 \times 10^{-2}$  M) that used to prepare the ANNP-based crystals. The reference results in Fig. 3a in the main text were acquired using this crystal, which indicated no detectable UC emission.

**Table S1.** Summary of the data acquired from 10 crystals after annealing (#A1–10) and 10 crystals before annealing (#B1–10).

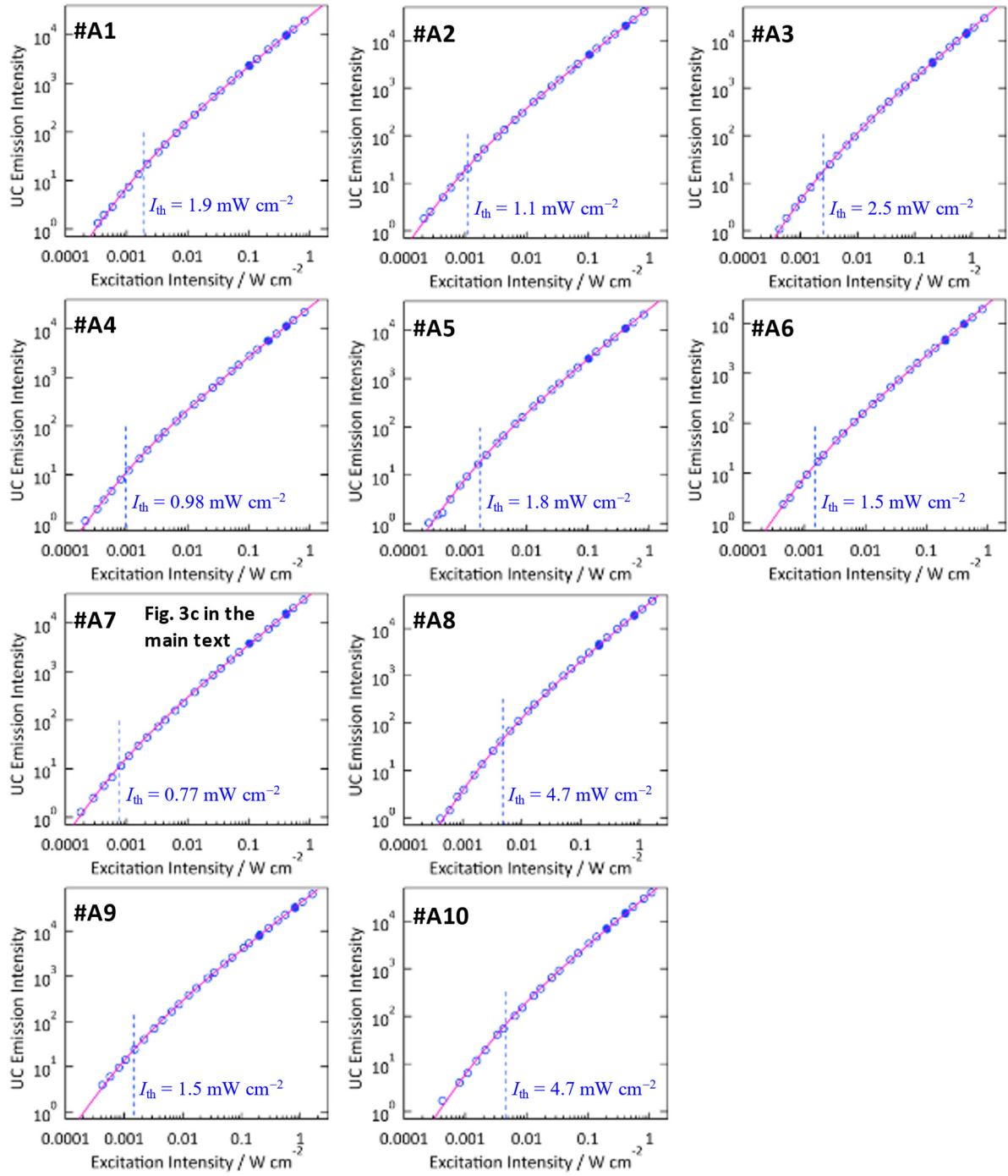
| Sample#        | $\Phi_{uc}^a$<br>/ % | $I_{th}$<br>/ mW cm <sup>-2</sup> | PtOEP concentration<br>/ 10 <sup>-5</sup> M | Crystal thickness<br>/ $\mu$ m |
|----------------|----------------------|-----------------------------------|---|--------------------------------|
| A1             | 16.4                 | 1.9                               | 3.5   | 138                            |
| A2             | 14.9                 | 1.1                               | 5.9   | 158                            |
| A3             | 14.2                 | 2.5                               | 3.8   | 102                            |
| A4             | 14.2                 | 0.98                              | 5.3   | 107                            |
| A5             | 13.8                 | 1.8                               | 5.2   | 133                            |
| A6             | 13.7                 | 1.5                               | 5.9   | 112                            |
| A7             | 12.9                 | 0.77                              | 4.1   | 135                            |
| A8             | 12.2                 | 4.7                               | 4.5   | 130                            |
| A9             | 11.4                 | 1.5                               | 7.7   | 120                            |
| A10            | 10.8                 | 4.7                               | 4.2   | 183                            |
| <b>Average</b> | 13.4                 | 2.1                               | 5.0 <sup>b</sup>                            | 132                            |

| Sample#        | $\Phi_{uc}^a$<br>/ % | $I_{th}$<br>/ mW cm <sup>-2</sup> | PtOEP concentration<br>/ 10 <sup>-5</sup> M | Crystal thickness<br>/ $\mu$ m |
|----------------|----------------------|-----------------------------------|---|--------------------------------|
| B1             | 6.2                  | 353                               | 5.6   | 162                            |
| B2             | 6.0                  | 226                               | 6.0   | 122                            |
| B3             | 5.7                  | 460                               | 4.4   | 197                            |
| B4             | 5.2                  | 722                               | 3.4   | 117                            |
| B5             | 4.8                  | 742                               | 8.6   | 56.5                           |
| B6             | 4.6                  | 282                               | 7.2   | 96.7                           |
| B7             | 4.5                  | 357                               | 4.7   | 70.3                           |
| B8             | 4.2                  | 1020                              | 3.6   | 56.5                           |
| B9             | 3.5                  | 266                               | 4.3   | 188                            |
| B10            | 3.4                  | 405                               | 3.4   | 233                            |
| <b>Average</b> | 4.8                  | 483                               | 5.1 <sup>b</sup>                            | 130                            |

<sup>a</sup> Definition of maximum 50%.

<sup>b</sup> This concentration corresponds to sensitizer:annihilator mole ratio of ca. 1:48000.



**Fig. S6.** Excitation intensity dependence of UC emission intensity measured for UC crystals after annealing, #A1–10 in Table S1. Here, the data represented by open marks were acquired first by increasing the excitation intensity, and then the data represented by filled marks were acquired to check the quantitative reproducibility.

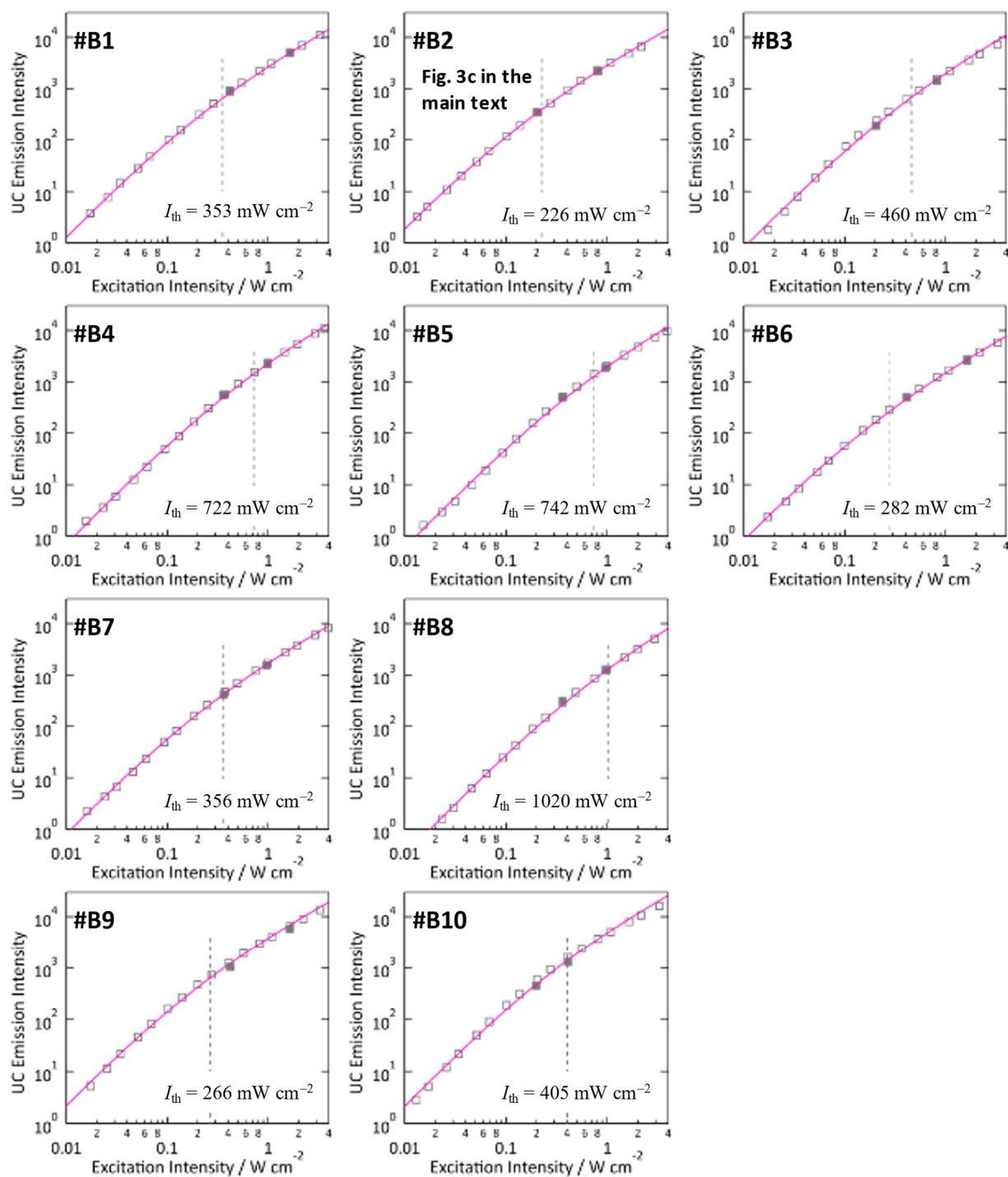


**Fig. S7.** Excitation intensity dependence of UC emission intensity measured for UC crystals before annealing, #B1–10 in Table S1. Here, the data represented by open marks were acquired first by increasing the excitation intensity, and then the data represented by filled marks were acquired to check the quantitative reproducibility.

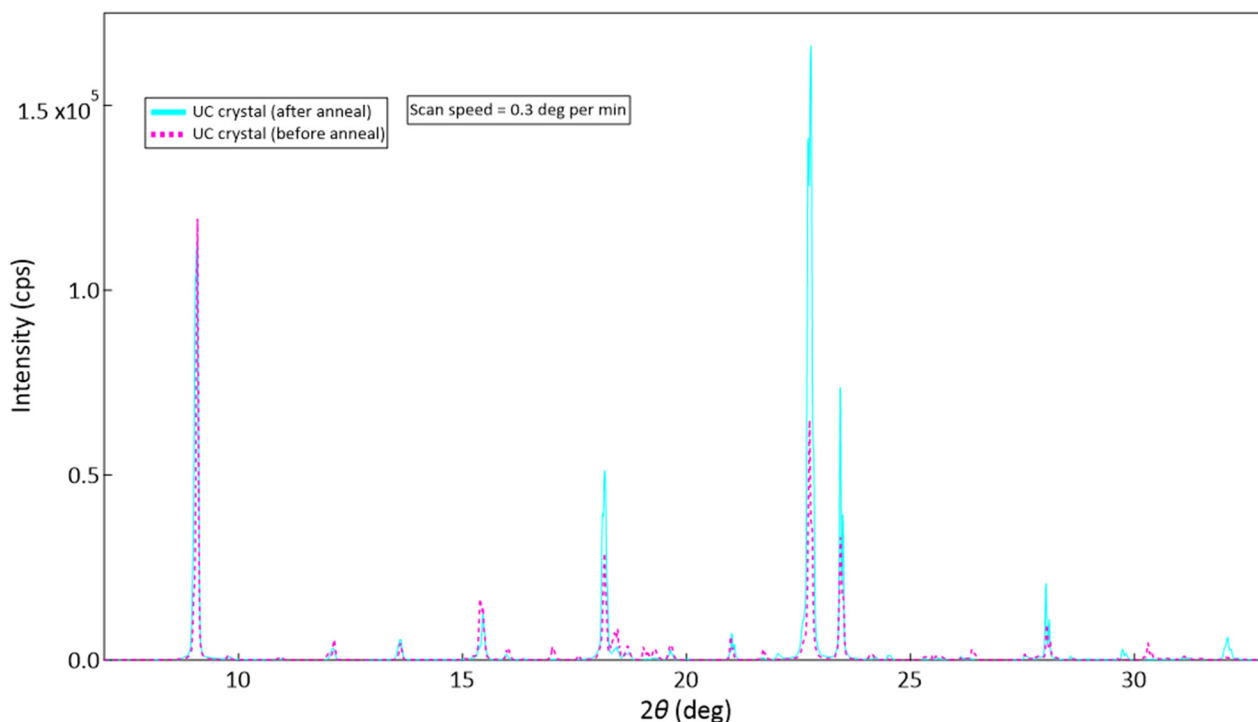


**Fig. S8.** Comparison of the powder-X-ray diffraction (PXRD) patterns acquired from the UC crystals before and after annealing. The patterns were acquired with an X-ray diffractometer (Rigaku, Smart-Lab) with Bragg–Brentano geometry. Before these measurements, the crystals were cut into fine powder with a razor blade to ensure the isotropic orientation of the crystal. The quantity of the sample as well as the measurement conditions were the same between these measurements and therefore the vertical axis values are intercomparable.

**Table S2.** Summary of the fluorescence quantum yields measured with an absolute photoluminescence quantum yield spectrometer.

| Sample type                               | $\Phi_{\text{FL}}$ , before anneal | $\Phi_{\text{FL}}$ , after anneal |
|---|------------------------------------|-----------------------------------|
| UC crystals                               | 38.7 %                             | 41.7 %                            |
| Reference crystals prepared without PtOEP | 44.5 %                             | 47.4 %                            |

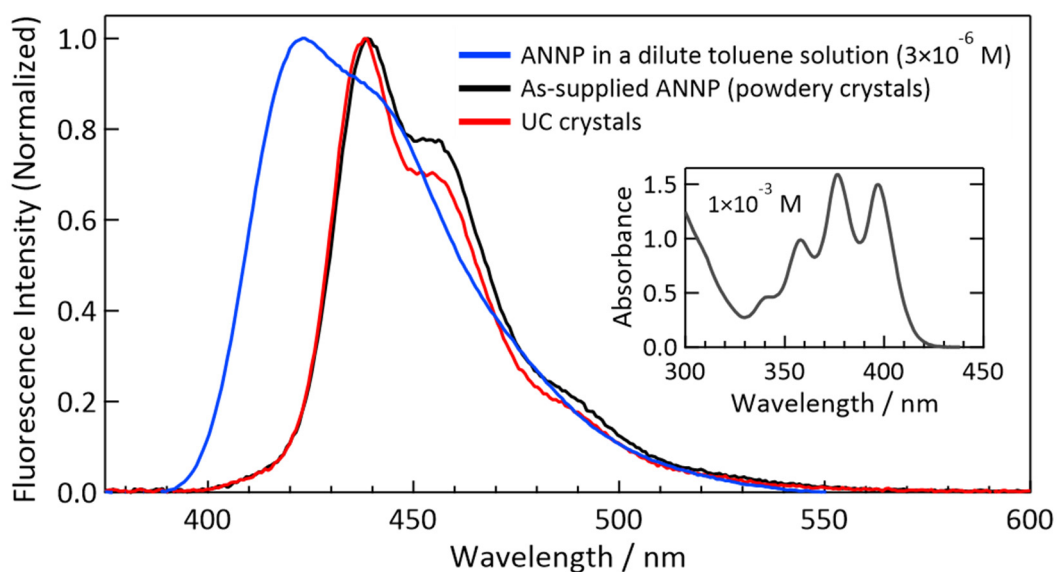


**Fig. S9.** Comparison of the fluorescence spectra of ANNP in a dilute toluene solution ( $3 \times 10^{-6}$  M, deaerated by three freeze-pump-thaw cycles), powdery crystals of as-supplied ANNP, and the UC crystals containing PtOEP, where the peak values have been normalized to 1. These spectra were acquired with a photoluminescence quantum yield spectrometer (Hamamatsu, C11347-01). Inset shows the absorption spectrum of ANNP in a toluene solution ( $1 \times 10^{-3}$  M, optical path length: 1 mm).

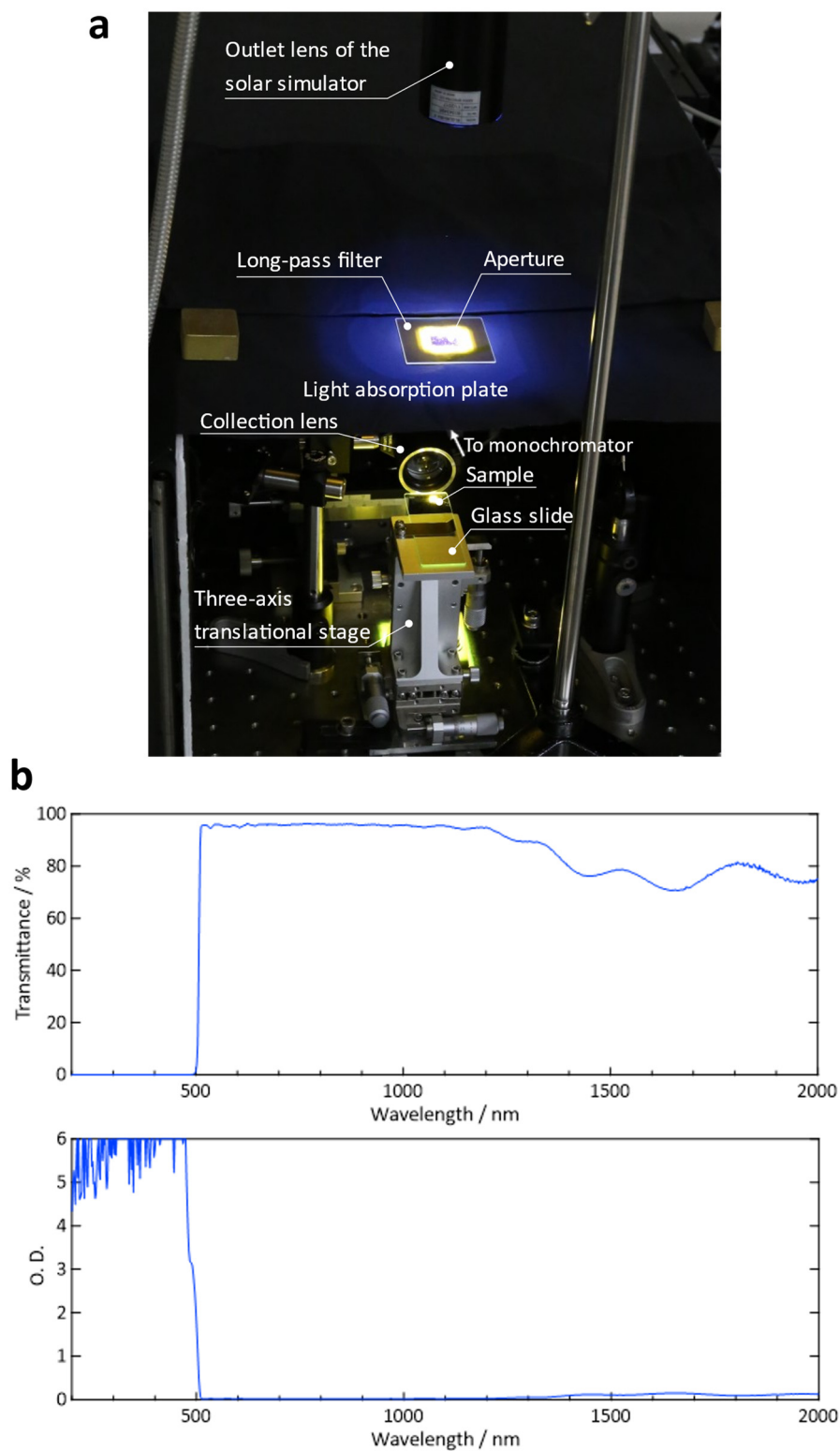


**Fig. S10.** (a) Photograph of the experimental setup with the solar simulator and (b) transmittance and optical density spectra of the 510-nm long-pass filter used. Refer to the Experimental section for details.

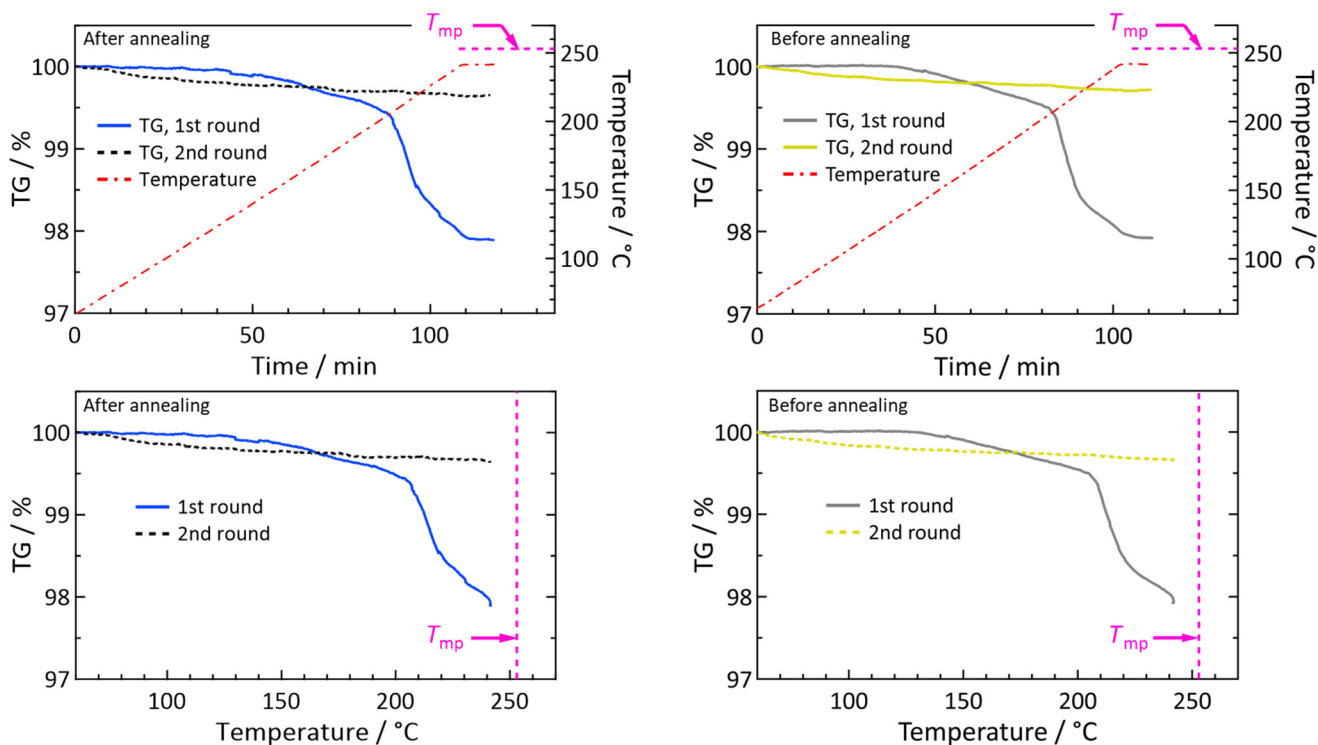


**Fig. S11.** TGA profiles of the UC crystals after (left) and before (right) annealing, acquired at a heating rate of 2°C/min and flowing 400 sccm of nitrogen gas. The melting point of ANNP ( $T_{mp}$ , 253 °C) is indicated in these panels. From the top panels where the TG values are plotted against time, decreases in the mass by ca. 2.1% were recognized, which we attribute to the included ethanol as indicated by the analysis of the single-crystal X-ray diffraction data (refer to Fig. 4b in the main text).

**Table S3.** Summary of the crystallographic data.

|                                | <b>As-supplied ANNP (sublimation grade)</b> | <b>ANNP crystal prepared without PtOEP</b> | <b>ANNP-UC crystal (before anneal)</b> | <b>ANNP-UC crystal (after anneal)</b> |
|--------------------------------|---|--|--|---------------------------------------|
| <b>Moiety formula</b>          | C40 H26                                     | C40 H26,<br>0.197(C2 H6 O)                 | C40 H26,<br>0.198(C2 H6 O)             | C40 H26,<br>0.198(C2 H6 O)            |
| <b>Formula weight</b>          | 506.61                                      | 515.68                                     | 515.73                                 | 515.73                                |
| <b>Temperature (K)</b>         | 93  | 93   | 93                                     | 93                                    |
| <b>Crystal system</b>          | Monoclinic                                  | Monoclinic                                 | Monoclinic                             | Monoclinic                            |
| <b>Space group</b>             | <i>I2/a</i>                                 | <i>I2/a</i>                                | <i>I2/a</i>                            | <i>I2/a</i>                           |
| <b>Z</b>                       | 8   | 8  | 8                                      | 8                                     |
| <b>a (Å)</b>                   | 18.9032(3)                                  | 18.8286(3)                                 | 18.8388(4)                             | 18.8241(3)                            |
| <b>b (Å)</b>                   | 7.4490(1)                                   | 7.4980(1)                                  | 7.4948(2)                              | 7.5014(2)                             |
| <b>c (Å)</b>                   | 38.5591(5)                                  | 38.7615(6)                                 | 38.7701(9)                             | 38.7559(8)                            |
| <b><math>\alpha</math> (°)</b> | 90  | 90   | 90                                     | 90                                    |
| <b><math>\beta</math> (°)</b>  | 96.953(1)                                   | 96.684(1)                                  | 96.653(2)                              | 96.531(2)                             |
| <b><math>\gamma</math> (°)</b> | 90  | 90   | 90                                     | 90                                    |
| <b>V (Å<sup>3</sup>)</b>       | 5389.58(13)                                 | 5435.03(14)                                | 5437.2(2)                              | 5437.1(2)                             |
| <b>R (%)</b>                   | 3.50  | 4.01                                       | 4.70                                   | 4.25                                  |
| <b>CCDC deposit number</b>     | 2109297                                     | 2109298                                    | 2109299                                | 2109300                               |

**Table S4.** Comparison of the diffusion properties of triplet excitons with those reported by some previous works of solid TTA-UC.

| Emitter                     | $D_T / \text{cm}^2 \text{s}^{-1}$ | $\tau_T / \text{ms}$ | Definition of $L_D$  | Z | $L_T / \text{nm}$ |
|-----------------------------|-----------------------------------|----------------------|----------------------|---|-------------------|
| ANNP<br>(present study)     | $9.22 \times 10^{-7}$             | 5.1                  | $\sqrt{2ZD_T\tau_T}$ | 3 | 1680              |
|                             |                                   |                      | $\sqrt{ZD_T\tau_T}$  | 3 | 1190              |
| MOF <sup>4</sup>            | $7.7 \times 10^{-6}$              | 3.2                  | $\sqrt{ZD_T\tau_T}$  | 1 | 1600 <sup>a</sup> |
| DPA <sup>5</sup>            | $6.43 \times 10^{-10}$            | 0.36                 | $\sqrt{ZD_T\tau_T}$  | 1 | 4.9               |
| Anthracene <sup>5</sup>     | $1.67 \times 10^{-7}$             | 0.15                 | $\sqrt{ZD_T\tau_T}$  | 1 | 50                |
| BFA-Ph (glass) <sup>6</sup> | $2.13 \times 10^{-9}$             | 1.374                | $\sqrt{2ZD_T\tau_T}$ | 3 | 41.9              |
| DPA (glass) <sup>7</sup>    | $2.2 \times 10^{-9}$              | 1.0                  | $\sqrt{ZD_T\tau_T}$  | 3 | 25.8              |

<sup>a</sup>: This value is much larger than the size of the material (ca. 55 nm).

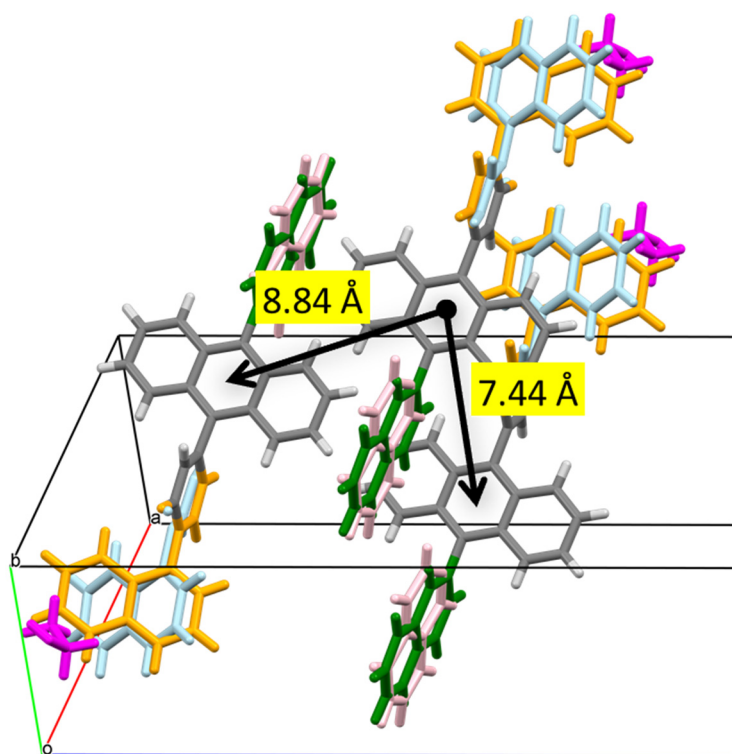


**Fig. S12.** Illustrations of the nearest-neighbor and second-nearest neighbor distances between adjacent ANNP molecules in the crystal. Refer to the caption in Fig. 4b in the main text for an interpretation of the colors.

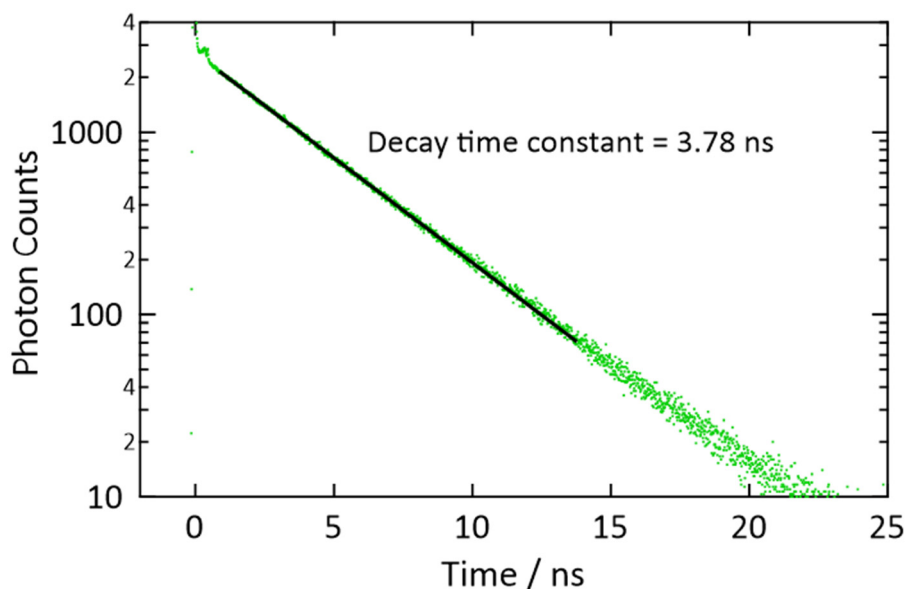


**Fig. S13.** Time-resolved fluorescence intensity decay curve for ANNP in a dilute toluene solution ( $3 \times 10^{-6}$  M, deaerated by three freeze-pump-thaw cycles; excitation: 405 nm, monitor: 440 nm). The black line is the curve fit by a single exponential decay function.

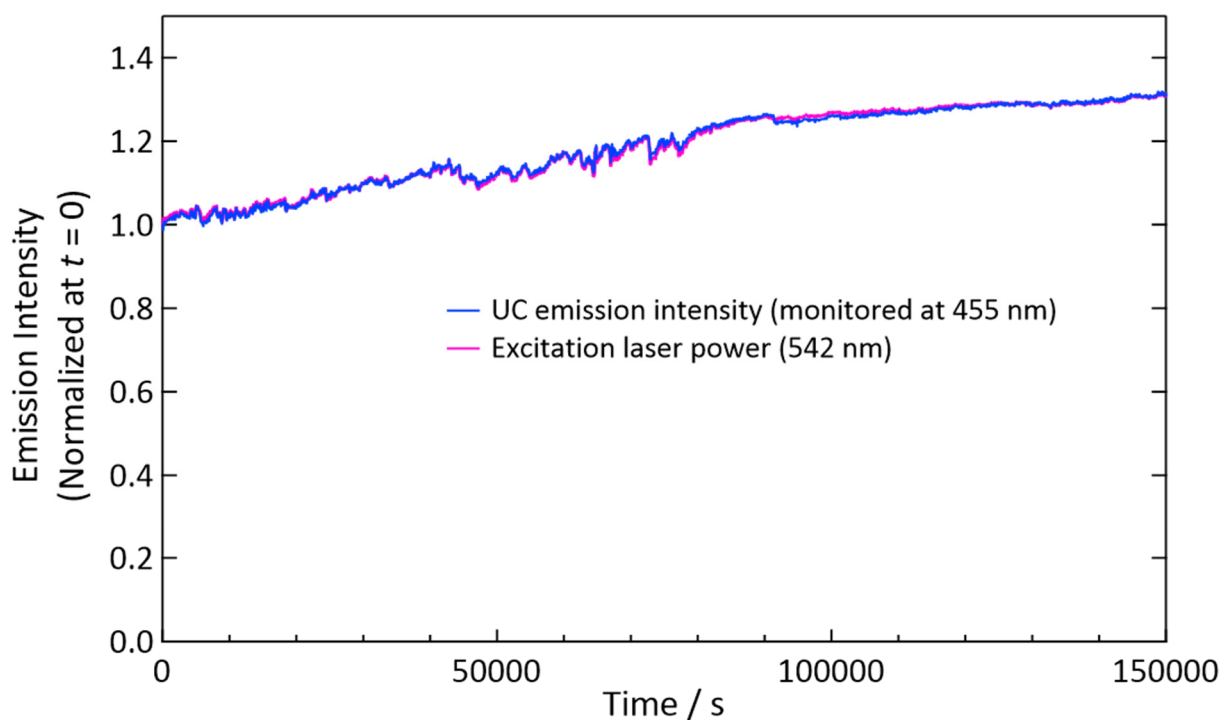


**Fig. S14.** Temporal fluctuation of the UC emission intensity (blue) and excitation laser power (pink) during the experiment of Fig. 3f shown in the main text. The excitation intensity was  $20 \text{ mW cm}^{-2}$ , which was approximately 10 times higher than  $I_{\text{th}}$  (see Table S1). This regime corresponds to the strong excitation limit<sup>2,3</sup> and therefore the UC emission intensity is proportional to the excitation laser power.

## References

- 1 J. N. Demas, G. A. Crosby, *J. Phys. Chem.*, **1971**, 75, 991–1024.
- 2 A. Haebele, J. Blumhoff, R. S. Khayzer and F. N. Castellano, *J. Phys. Chem. Lett.*, **2012**, 3, 299–303.
- 3 Y. Murakami and K. Kamada, *Phys. Chem. Chem. Phys.*, **2021**, 23, 18268–18282.
- 4 J. Park, M. Xu, F. Li and H. C. Zhou, *J. Am. Chem. Soc.*, **2018**, 140, 5493–5499.
- 5 K. Narushima, S. Hirata and M. Vacha, *Nanoscale*, **2017**, 9, 10653–10661.
- 6 S. Raišys, O. Adomėnienė, P. Adomėnas, A. Rudnick, A. Köhler and K. Kazlauskas, *J. Phys. Chem. C*, **2021**, 125, 3764–3775.
- 7 S. Raišys, K. Kazlauskas, S. Juršėnas and Y. C. Simon, *ACS Appl. Mater. Interfaces*, **2016**, 8, 15732–15740.